Model-Based Projections and Uncertainties of Near-Surface Wind Climate in Western Canada

Jeffrey T. Daines, Adam H. Monahan, and Charles L. Curry

October 2016

Model-Based Projections and Uncertainties of Near-Surface Wind Climate in Western Canada

JEFFREY T. DAINES, ADAM H. MONAHAN, AND CHARLES L. CURRY

University of Victoria, Victoria, British Columbia, Canada

(Manuscript received 22 February 2016, in final form 3 August 2016)

ABSTRACT

Near-surface wind is important in forestry, agriculture, air pollution, building energy use, and wind power generation. In western Canada it presently plays a minor role in power generation, but ongoing reductions in the cost of wind power infrastructure and the increasing costs of conventional power generation (including environmental costs) motivate the assessment of the projected future wind climate and uncertainties in this projection. Multiple realizations of the Canadian Regional Climate Model (CRCM) at 45-km resolution were driven by two global climate models over the periods 1971–2000 (using historical greenhouse gas concentrations) and 2031–60 (using the SRES-A2 concentration scenario). Hourly wind speeds from 30 stations were analyzed over 1971–2000 and used to calibrate downscaled ensembles of projected wind speed distributions over 2031–60. At most station locations modest increases in mean wind speed were found for a majority of the projections, but with an ensemble spread of the same order of magnitude as the increases. Relative changes in mean wind speeds at station locations were found to be insensitive to the station observations and calibration technique. In view of this result, projected relative changes in future wind climate over the entire CRCM domain were estimated using uncalibrated pairs of past-period and future-period wind speed distributions. The relative changes are robust, in the sense that their ensemble mean relative change is greater than their standard deviation, but are not very substantial, in the sense that their ensemble mean change is generally less than the standard deviation of their annual means.

1. Introduction

The western Canadian provinces of Alberta and British Columbia encompass a diverse range of surface characteristics, from the Pacific Ocean on the west to the Canadian prairies in the east, separated by mountain ranges, high plateaus, and deep river valleys (Fig. 1). Electrical power is generated primarily from fossil fuels in Alberta and hydropower in British Columbia (Alberta Energy 2015; EnergyBC 2016). Fossil fuel use in Alberta may eventually be reduced in response to climate change concerns, so increased energy from other sources will be required. The most recent hydroelectric dam approved by the government of British Columbia may be the last (Eagland 2015), so further generating capacity will eventually be needed in that province as well. Considering the future generation of electrical power in the two provinces together makes sense, particularly if they were to cooperate to reduce overall use of fossil fuels (Scorah et al. 2012; Sopinka 2012).

Wind energy generation is expanding rapidly worldwide and has already been developed in Alberta and British Columbia (2015 installed capacities of 1471 and 488.7 MW, respectively; Canadian Wind Energy Association 2015). Both the expansion of existing wind farms and new construction should take into account the possibility that anthropogenic climate change could alter the wind climate and its variability. The overall goal of this study is to estimate future changes in the wind climate in this region and the uncertainties associated with these projections, particularly those arising from natural (internal) variability. The effect of natural variability on future temperature and precipitation projections has been considered elsewhere (Deser et al. 2012).

Global climate models (GCMs) can be used to simulate wind speeds near the surface but have a coarse spatial resolution that poorly represents features like topography that strongly influence wind variability in

Corresponding author address: Jeffrey T. Daines, School of Earth and Ocean Sciences, University of Victoria, P.O. Box 3065 STN CSC, Victoria, BC V8W 3V6, Canada.
E-mail: jtdaines@uvic.ca

DOI: 10.1175/JAMC-D-16-0091.1

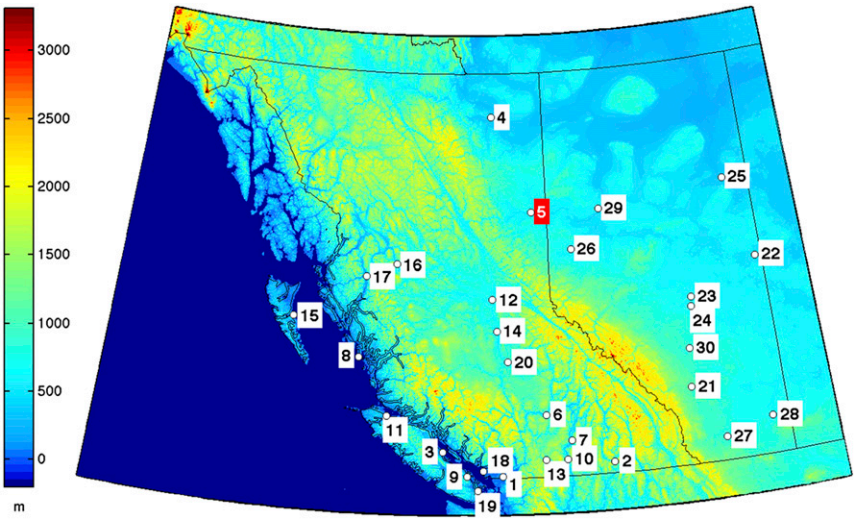

FIG. 1. Topographic map of British Columbia and Alberta using 1-arc-min-resolution elevations (m) from ETOPO1 (Amante and Eakins 2009) showing the EC weather station locations enumerated as in Table 1. Map borders are 48° and 61°N and 140° and 108°W. The station with a red marker is Fort St. John (station 5), referred to as a representative station in the text.

western Canada. Desirable wind turbine sites such as mountain ridges are completely missed by the smoothed topography used in GCMs. To estimate regional wind climate from GCMs, there are two main methods (and some hybrids) used to downscale winds from GCMs to a regional scale. Statistical downscaling uses statistical relationships between local observations and large-scale GCM variables (Breslow and Sailor 2002; Mansbach and Cayan 2010; Sailor et al. 2008; Curry et al. 2012; Culver and Monahan 2013), while in dynamical downscaling a relatively high-resolution regional climate model (RCM) is driven over the subregion of interest by a global-scale model (Laprise 2008; Rasmussen et al. 2011; Pryor et al. 2012). In this study dynamical downscaling results from multiple RCM simulations driven by two GCMs are used to estimate future changes in wind climate in British Columbia and Alberta. Dynamical downscaling has been used for projecting temperature and precipitation in this region (Plummer et al. 2006; Casati and de Ela 2014; Mladjic et al. 2011) and nearby in the U.S. Pacific Northwest (Salathé et al. 2008), but dynamical downscaling of the wind climate was not examined in those studies. Elsewhere, dynamical downscaling has been used to study the future wind climate of the contiguous United States (Pryor et al. 2009, 2012) and Europe (Pryor et al. 2005). It has also been used to project future changes in wind speed in wind farm regions in California (Rasmussen et al. 2011).

Despite their finer resolution, RCM simulations are generally biased, and past observations are needed for calibration to remove systematic errors (Ho et al. 2012). Different approaches to calibration exist, and these generally yield different results. Calibration relies on observational data such as those provided by weather stations. There are only 30 weather stations in Alberta and British Columbia for which long-term near-surface hourly wind speed data are available, and these data are of variable quality (Wan et al. 2010).

Beyond uncertainties in projections resulting from different calibration approaches and mixed-quality station data, further uncertainties result from differences between the driving GCMs, resolution sensitivity of RCM simulations, and natural internal variability of the climate system. A primary goal of this study is to assess the relative magnitudes of these uncertainties in projections of near-surface wind speeds and wind power in Alberta and British Columbia. We will demonstrate that, at least in this region, estimates of relative changes in wind speed and power are relatively insensitive to the calibration methods applied and therefore to the quality of observational data, although the other uncertainties remain. In particular, our work can be considered an extension of that of Deser et al. (2012), who probed the uncertainty in future temperature and precipitation projections due to internal variability alone, to the realm of wind climate, albeit over a limited region. Because only a single RCM is considered, this study does not address uncertainties in projections associated with the use of different downscaling models as is considered in, for example, Pryor et al. (2012).

The primary goal of the work reported upon in this paper is not to compare results with other regional

downscaling work, but rather to use one regional climate model run multiple times in combination with two global climate models using the same emissions scenario so as to attempt to isolate the effects of calibration and internal variability in the models on the projected wind climate.

This study is organized as follows. Section 2 provides a description of the simulations and observational data used to calibrate them. In section 3, the calibration methods applied to the output of the Canadian Regional Climate Model (CRCM) driven by two GCMs are described. In section 4, the projected future wind climate in the region is estimated using the calibrated wind speeds. As part of this analysis, we also estimate relative change in the wind climate over the entire region, not only at the station locations. Section 5 assesses the relative importance of the various uncertainties in the projection of future wind climate. The main conclusions of the work are summarized in section 6.

2. Data and models

This section introduces the climate model simulations used to estimate future wind climate in the region and the observational data used to calibrate the simulations. For this study, observational data and simulated winds from climate models were obtained as wind speeds at a nominal height of 10 m (which we will refer to as near surface). Because long records of winds above 10 m are not available for calibration of model simulations in our study domain, our focus will be on 10-m wind speeds.

a. Dynamical downscaling

The CRCM, version 4.2.4, is used as a downscaling tool in this study (Caya and Laprise 1999; Mladjic et al. 2011). Simulations are considered in which the CRCM is driven by 1) the European Centre for Medium-Range Weather Forecasts (ECMWF) ERA-40 global reanalysis, 2) the ECHAM5 global coupled climate model (from ECMWF), and 3) the Canadian Coupled Global Climate Model (CGCM3) model from the Canadian Centre for Climate Modelling and Analysis (CCCma). Simulations using the ECHAM5 and CGCM3 models are driven by historical (1958–2000) concentrations of long-lived greenhouse gases until the year 2000, when they switch to the SRES-A2 scenario (Nakićenović and Swart 2000), but they are otherwise freely evolving (i.e., not constrained by reanalysis for the historical period). Ensembles of three realizations of ECHAM5 and five realizations of CGCM3 were analyzed. The simulations analyzed here represent an ''ensemble of opportunity,'' insofar as they were generated as part of a different project meant to investigate the sensitivity of climate and hydrology to CRCM ensemble size and resolution over western Canada (Curry et al. 2016a,b).

We focus on a subregion of 38×44 grid points roughly between 48° and 61°N, and 140° and 108°W, as simulated by the CRCM at 45-km resolution (true at 60°N; Fig. 2). The CRCM simulation driven by the ERA-40 global reanalysis for the period 1973–2001 provides an estimate of the recent near-surface wind climate in the region. Time-mean near-surface wind speeds from the simulation shown in Fig. 2 provide a basis for considering where relative changes in the future wind climate may be important for the viability of wind farms. The minimum annual-mean 10-m wind speed for such development has been estimated to be 5.1–5.6 $m\,s^{-1}$ (National Renewable Energy Laboratory 2014). The dark contour in Fig. 2 identifies regions of the model domain where the mean wind speed exceeds 5 $m\,s^{-1}$. Existing wind farms are located in regions that have simulated mean wind speeds in excess of 5 $m\,s^{-1}$, with the exception of those south of Fort St. John, British Columbia (station 5 in Fig. 1).

The wind speeds obtained from the simulations driven by freely running GCMs were means of the model output calculated at either the 3-hourly (CGCM3) or 6-hourly (ECHAM5) archiving interval of the respective run.

b. Observational data

In this study, simulated wind speeds obtained from the CRCM driven by both GCMs are calibrated using observed hourly near-surface wind speed data from 30 weather stations in the provinces of Alberta and British Columbia downloaded from Environment Canada (EC) (http://climate.weather.gc.ca/historical_data/search_historic_data_e.html). Those stations are the only stations with raw hourly wind speeds from 1953 to the present for which EC also provides monthly mean wind speeds (in most cases from 1953 to 2011) that have been adjusted (homogenized) for equipment, location, and environmental changes. The 30 stations are identified in Fig. 1, while Table 1 lists the station names and their latitudes, longitudes, and elevations as provided by EC. With one exception (McInnes Island), all of the stations are located at airports. Fort St. John (station 5), indicated with a red marker in Fig. 1, will be used throughout this study as a representative example to illustrate the procedure used to calibrate simulation results at the station locations using observations.

The archived hourly wind speeds at the stations were constructed from 1-min mean wind speeds ending at the reported time of the observation for years prior to 1996 and 2-min mean wind speeds since 1996, with speeds recorded to the nearest knot since 1996 and the nearest statute mile per hour prior to 1996 (Wan et al. 2010).

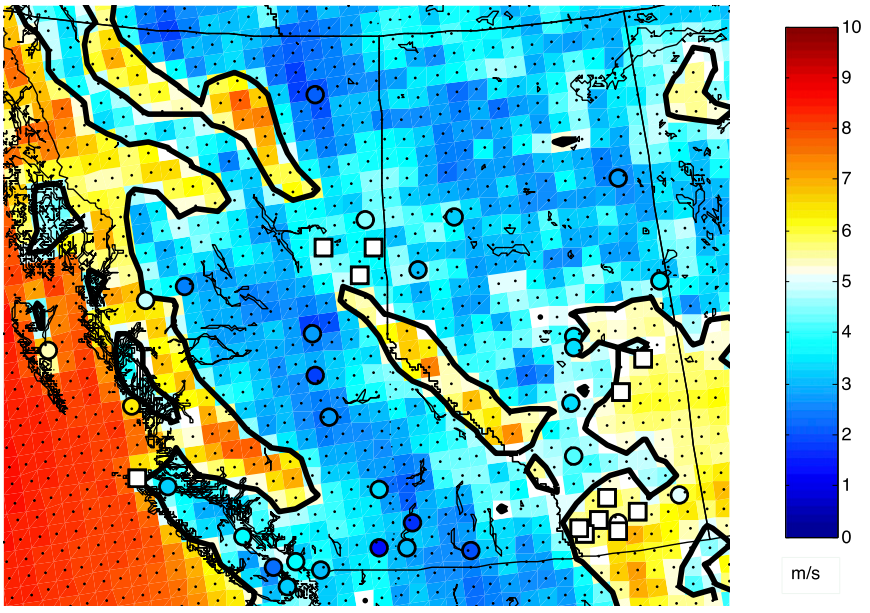

FIG. 2. Mean near-surface wind speeds for 1973–2001 from the CRCM driven by the ECMWF ERA-40 global reanalysis shown for 45-km square grid boxes including the portion of the grid covering the provinces of Alberta and British Columbia. The grid is indicated by small black dots at the center of each grid box. The heavy black line is the 5 m s^{-1} contour. The EC weather stations enumerated in Fig. 1 are indicated by colored circles depicting observed mean wind speeds. White squares indicate the locations of existing wind farms.

However, the data provided by EC are in integer kilometers per hour. As a result of these multiple steps of rounding, no observations are reported for some discrete speed values (in km h^{-1}) within the observed range. Further, the time series of hourly wind speeds also contain a large number of zero and missing wind speeds for some of the stations. Recent observations at the stations using sonic anemometers, rather than the cup anemometers used for the 1971–2000 observations, contain fewer zero speed records and an increased frequency of 1–3 km h^{-1} speeds. It is likely that the zeros reported by the cup anemometers represent low wind speeds that should be retained in the hourly wind speed time series. Before averaging over 3- and 6-h periods to form time series for the calibration of the simulated wind speeds, each raw hourly wind speed was multiplied by the ratio of the homogenized monthly mean wind speed obtained from EC to the raw monthly mean for the relevant month. The resulting 3- and 6-h mean wind speeds used for calibration therefore have monthly means equal to the homogenized monthly means. A more detailed discussion of the processing of the data is presented in Daines (2015). We also investigated the use of the North American Regional Reanalysis (NARR; Mesinger et al. 2006) as an alternative pseudo-observational dataset, but chose not to use it because of problematic aspects of its representation of surface winds in this region (Daines 2015). As shown in Pryor et al. (2009), near-surface winds speeds obtained from reanalysis products can differ substantially. Hence they may not be suitable for use in place of observations in the calibration of model output.

c. *Simulated and observed winds at a representative station: Fort St. John*

In the upper panels of Fig. 3, kernel density estimates of distributions of CRCM-simulated wind speed for 1971–2000 (in red) and 2031–60 (in black) interpolated to Fort St. John are plotted along with the 1971–2000 histogram estimates (in green) of corrected mean station wind speed distributions. Bilinear interpolation using the four nearest grid points to the station location was used. A separate curve is plotted for each ensemble member. The distributions of the simulated wind speeds for the two time periods are so similar that the 2031–60 curves lie close to or on top of the 1971–2000 curves. From Fig. 3, it is clear that the simulated wind speed distribution shows only modest variability among ensemble members, differences between driving GCMs, and change between the recent past and the mid-twenty-first century. Further, the relative frequency of CRCM-simulated wind speeds is biased low relative to observations at speeds between 3 and 5 m s^{-1} and biased high above 7 m s^{-1}.

TABLE 1. Station numbers for Fig. 1, names, locations (lat °N and lon °W) and elevations (m) of all stations in British Columbia and Alberta with hourly raw wind speeds and monthly homogenized wind speed data available from EC.

No.	Station name	Province	Lat (°N)	Lon (°W)	Elev (m)
1	Abbotsford Airport	BC	49.03	122.36	59.1
2	Castlegar Airport	BC	49.30	117.63	495.0
3	Comox Airport	BC	49.72	124.90	26.0
4	Fort Nelson Airport	BC	58.84	122.60	382.0
5	Fort St John Airport	BC	56.24	120.74	695.0
6	Kamloops Airport	BC	50.70	120.44	345.0
7	Kelowna Airport	BC	49.96	119.38	429.5
8	McInnes Island	BC	52.26	128.72	26.0
9	Nanaimo Airport	BC	49.05	123.87	28.0
10	Penticton Airport	BC	49.46	119.60	344.0
11	Port Hardy Airport	BC	50.68	127.37	22.0
12	Prince George Airport	BC	53.89	122.68	691.0
13	Princeton Airport	BC	49.47	120.51	700.0
14	Quesnel Airport	BC	53.03	122.51	545.0
15	Sandspit Airport	BC	53.25	131.81	6.0
16	Smithers Airport	BC	54.82	127.18	522.0
17	Terrace Airport	BC	54.47	128.58	217.0
18	Vancouver International Airport	BC	49.20	123.18	4.0
19	Victoria International Airport	BC	48.65	123.43	19.0
20	Williams Lake Airport	BC	52.18	122.05	940.0
21	Calgary International Airport	AB	51.11	114.02	1084.0
22	Cold Lake Airport	AB	54.42	110.28	541.0
23	Edmonton City Centre Airport	AB	53.57	113.52	671.0
24	Edmonton International Airport	AB	53.32	113.58	723.0
25	Fort McMurray Airport	AB	56.65	111.22	369.0
26	Grande Prairie Airport	AB	55.18	118.89	669.0
27	Lethbridge Airport	AB	49.63	112.80	929.0
28	Medicine Hat Airport	AB	50.02	110.72	717.0
29	Peace River Airport	AB	56.23	117.45	571.0
30	Red Deer Airport	AB	52.18	113.89	905.0

We repeated the analysis behind Fig. 3 for all 30 station locations using the nearest grid point to assign values instead of bilinear interpolation. At a majority of stations, the degree to which the uncalibrated distributions fit the observed wind speed distribution did not depend upon which method was used to estimate simulated distributions at the station location. Where differences were observed, the fits were better for the interpolated data as often as for the nearest grid point data.

d. Wind power density

According to Betz's law (Manwell et al. 2012), the maximum energy that an ideal wind turbine can capture from the wind is 59.3% of the wind power density (WPD), which is calculated as

$$\mathrm{WPD} = \frac{1}{2}\rho V^3,$$

where ρ is the air density and V is the instantaneous wind speed. Because of the cubic relationship between wind power density and speed, the model bias at higher wind speeds will have an enhanced effect on the simulated extractable energy. This problem can be addressed by calibrating the simulated wind speeds using observed distributions of wind speed to remove bias. Throughout this study, wind power density is estimated from the time series of calibrated simulated wind speeds using the highest time resolutions available, before taking a long-term mean. Climate model simulation results are available as 3- or 6-hourly means, depending on the driving model of the CRCM. Hence the wind power density may be underestimated, depending upon the time scale of the variability, as the CRCM archiving intervals smooth high-frequency variability of the wind. Further, a constant air density was assumed in calculating wind power density. Variations in air density are expected to contribute substantially less than variations in speed to power density variability.

3. Calibration of climate model simulations

a. Calibration using bias correction and change factor pathways

Calibration of climate projections uses statistical approaches to reduce model biases. Calibration has most

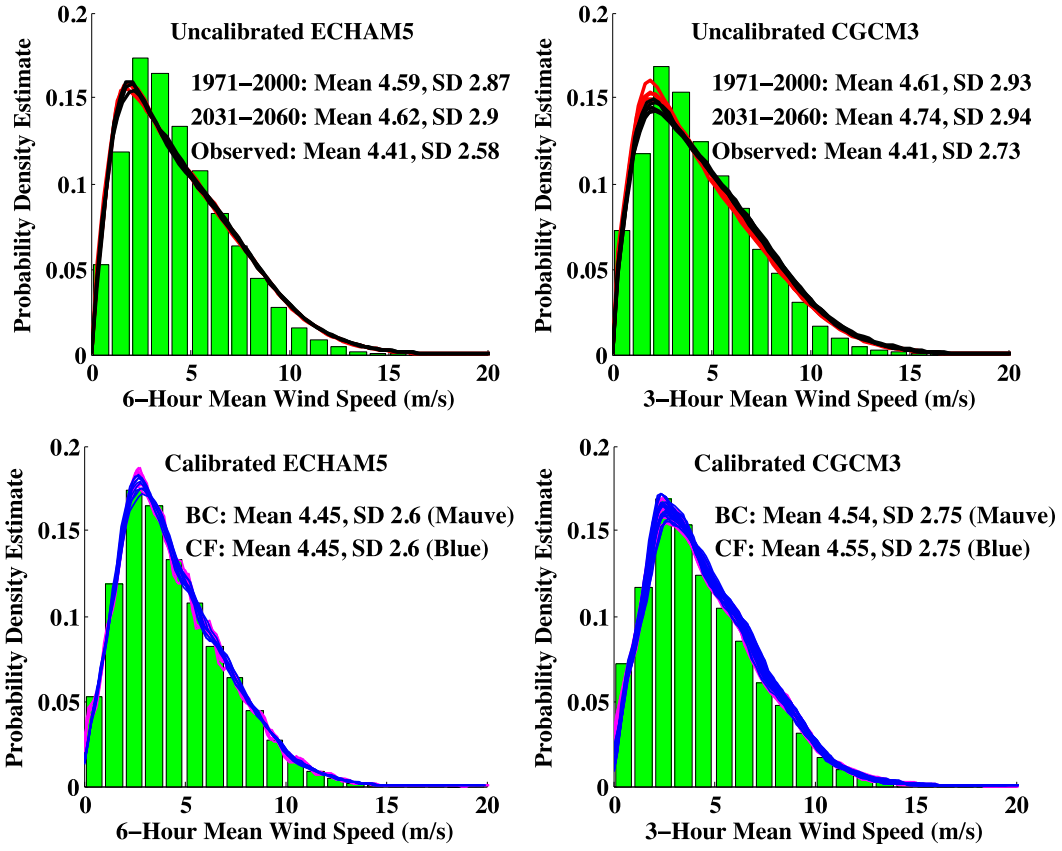

FIG. 3. Histograms of an estimate of the 1971–2000 probability density function of corrected and time-averaged observed hourly station wind speed distributions (green bars) at Fort St. John. Observations are (left) 3-h means and (right) 6-h means. (top) The histograms are overlaid by kernel density estimates of uncalibrated GCM-driven CRCM-simulated wind speed distributions for 1971–2000 (red curves) and 2031–60 (black curves) interpolated to Fort St. John. (bottom) The curves are the calibrated GCM-driven CRCM wind speed distributions for 2031–60 using BC (purple curves) and CF (blue curves) calibration pathways. The ECHAM5-driven (CGCM3-driven) ensemble members are plotted in the left (right) panel. Means are ensemble means of the time means, and SDs are ensemble means of the temporal standard deviations.

often been done in the context of surface temperature or precipitation (Piani et al. 2010; Haerter et al. 2011; Diaz-Nieto and Wilby 2005). As discussed in Ho et al. (2012), two distinct approaches to calibration are possible. The statistical relationship between past simulations and past observations can be applied to future simulations to obtain calibrated future simulations (bias correction pathway). Alternatively, the statistical relationship between past simulations and future simulations can be applied to past observations to obtain calibrated simulations (change factor pathway). There is no a priori reason to choose one pathway over the other, and the two calibration pathways generally result in different calibrated projections.

In the present study, two ensembles of simulations are considered, one with three members (the ECHAM5-driven simulations), and the other with five members (the CGCM3-driven simulations), each providing both historical (1971–2000) and future (2031–60) simulated wind speed distributions. As illustrated in Fig. 3, there are modest differences between the RCM-simulated wind speed distributions obtained using these two driving models. Hence, in the following, ensembles from each driving GCM will be dealt with separately. In addition, internal model variability results in differences between the realizations driven by the same GCM.

From the three ECHAM5-driven historical simulations and the historical observations, there are three possible transfer functions in the bias correction (BC) calibration pathway and nine in the change factor (CF) pathway, resulting from combining each historical simulation with each future simulation. This interchanging of past and future simulations assumes that the internal memory of variability is sufficiently short relative to the 30-yr separation of the past and future periods that each future 30-yr period is a possible partner to each past

30-yr period. As a result, each of the three BC transfer functions can be applied to any of the three future simulated distributions, giving nine calibrated future states. Similarly, nine CF transfer functions are obtained because each of the three historical period simulations could result in any one of the three future period simulations. For the CGCM3-driven simulations, the same reasoning results in 25 projected future wind speed distributions for each calibration pathway resulting from the various combinations of five historical and five future simulations. In each case, these combinations broaden the spread of the ensemble of future projections.

b. *Transfer functions: Q–Q matching versus power-law transforms*

Both the BC and CF calibration pathways require a statistical model to carry out the calibration, referred to as a transfer function. In this study two possible forms of transfer function were considered: 1) power-law transformations assuming that both the observed and simulated wind speed distributions can be described by Weibull distributions and 2) quantile–quantile (Q–Q) matching.

1) POWER-LAW TRANSFORMATION ASSUMING WEIBULL DISTRIBUTIONS

The two-parameter Weibull distribution is the most common parametric distribution presently used for empirical modeling of wind speed (Monahan 2014). In the present region of interest, Curry et al. (2012) used the Weibull distribution as an approximation to the observed histogram of wind speeds over British Columbia. If the observed wind speeds were found to be characterized well by the Weibull distribution, this distribution could be used for the calibration of projected wind speeds using the power-law transformation as described in Tye et al. (2014). Although Tye et al. (2014) used this transformation for high wind speeds only, it is a general mathematical result that can be used to map between any two Weibull-distributed quantities.

To test how well a power-law transformation assuming Weibull distributions would work as a transfer function for wind speed calibrations, an ensemble of five BC transfer functions were estimated for the CGCM3-driven simulations over 1971–2000. These transfer functions were then applied to the same 1971–2000 CGCM3-driven simulations, and the statistics of the resulting ''calibrated'' simulations were compared with the 1971–2000 observations. The result should ideally be an ensemble of debiased distributions whose statistics are symmetrically distributed around the observed values, normalized to a value of one in Fig. 4. This was the case for the mean speed, but not for the standard deviation of the mean speed, the 95th and 99th percentile speeds or the wind power density mean and standard deviation (gray dots). The biases in this calibration approach result from the fact that both the observed and simulated wind speed distributions deviate from the Weibull distribution. With only two parameters, the Weibull distribution is not able to capture the tail behavior of the wind speed distribution with sufficient accuracy for these data.

2) QUANTILE–QUANTILE MATCHING

Quantile–quantile matching avoids the assumption of a parametric probability distribution and has been employed in calibration of wind speeds (Michelangeli et al. 2009). It can be explained with an example for a BC calibration. A set of quantiles bounded by 0 and 100 is chosen, in increments of one. The observed speeds and historical simulated speeds at each of the quantiles are found. For each future simulated speed that needs to be calibrated, the quantiles (the upper and lower quantiles) corresponding to the values of the historical simulated speeds bracketing the future speed are found. The desired calibrated future speed is then obtained by linear interpolation between the observed speeds at those quantiles. This approach constitutes a transfer function. A similar procedure is used for the CF calibration.

One limitation of Q–Q matching is that there will be undetermined speeds in the calibrated distribution if the range of simulated future wind speed values exceeds that of the simulated historical wind speed values for the BC calibration pathway or the range of the observed wind speeds exceeds that of the simulated historical wind speed values for the CF pathway. We address this ambiguity by setting such undetermined wind speeds in the calibrated distribution to the value corresponding to the maximum speed in the observed distribution in the case of a BC calibration and to the maximum speed in the simulated future distribution in the case of CF calibration. This approximation was necessary in very few cases for the distributions studied.

As noted by Ho et al. (2012), another difficulty of Q–Q matching is that datasets with many data points of equal value can be problematic if simple interpolation is used between percentiles. This difficulty is an issue for the observed wind speeds here because of the rounding of observed values to integers discussed in section 2. To address this issue, a small random number between -0.01 and $+0.01\,\mathrm{m\,s^{-1}}$ was added to all observed wind speeds.

A comparison of observed and calibrated wind speed statistics obtained using Q–Q matching is also shown in

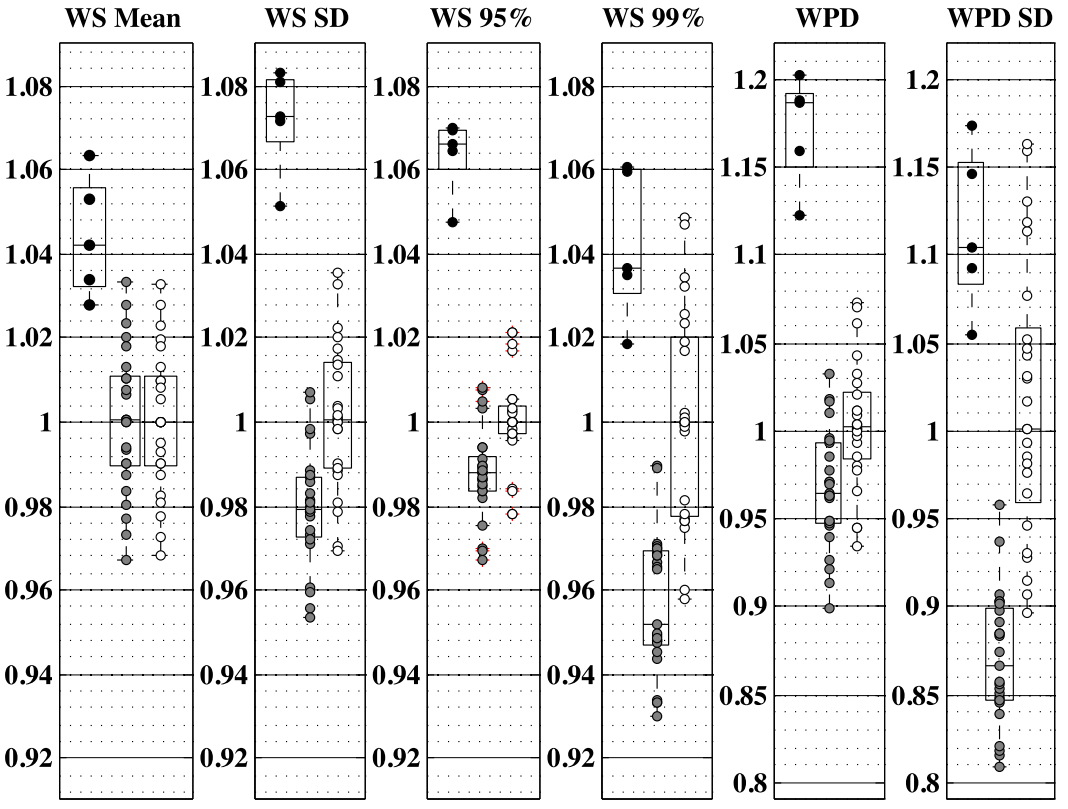

FIG. 4. Comparison of transfer functions using Q–Q matching and power-law transformations assuming Weibull distributions applied to 1971–2000 CGCM3-driven simulated wind speed distributions at Fort St. John, all normalized to observed 1971–2000 winds statistics. In the column headers, wind speed is WS, wind power density is WPD, standard deviation is SD, and the 95th and 99th percentiles are 95% and 99%, respectively. Black dots represent 1971–2000 simulated wind speed means, gray dots represent simulated wind means debiased using power-law transformations corresponding to the Weibull distribution, and white dots represent simulated wind means debiased using Q–Q matching. Individual dots correspond to individual ensemble members. In the box plot for each ensemble, the central mark is the median and the edges of the box are the 25th and 75th percentiles of each ensemble. The range on the vertical axis is different for the wind power statistics.

Fig. 4. The statistics of the distributions debiased using Q–Q matching (white dots) are roughly symmetric about the observed statistics (indicated by symmetry about the value of one). In contrast to the power-law transformation assuming Weibull distributions, the Q–Q matching transfer function results in a much better calibration for these data. While this result is shown only for Fort St. John in Fig. 4, similar results hold for all 30 stations.

4. Results

a. Q–Q matching applied to GCM-driven CRCM simulations

The lower panels of Fig. 3 illustrate kernel density estimates of simulated wind speed probability density functions for 2031–60, interpolated to Fort St. John, calibrated using observed wind speeds. In the final calculations, 10 001 quantiles were used (0 to 100 by 0.01); a sensitivity analysis demonstrates that the results are not qualitatively affected by an increase in the number of quantiles. The histogram of observed speeds, provided for comparison, shows that the projected future changes in the wind speed distribution are small for both the BC and CF pathways, a result similar to that found elsewhere in North America in other regional climate model simulations (Pryor et al. 2012; Rasmussen et al. 2011). The difference in means between the CGCM3-driven and ECHAM5-driven simulations is larger than the difference between the means from the BC and CF pathways. At Fort St. John, the estimate of mean wind power density obtained from calibrated wind speeds interpolated from model grid points differed by less than 1% from those obtained using nearest-neighbor grid points. Similarly small differences were found at other stations.

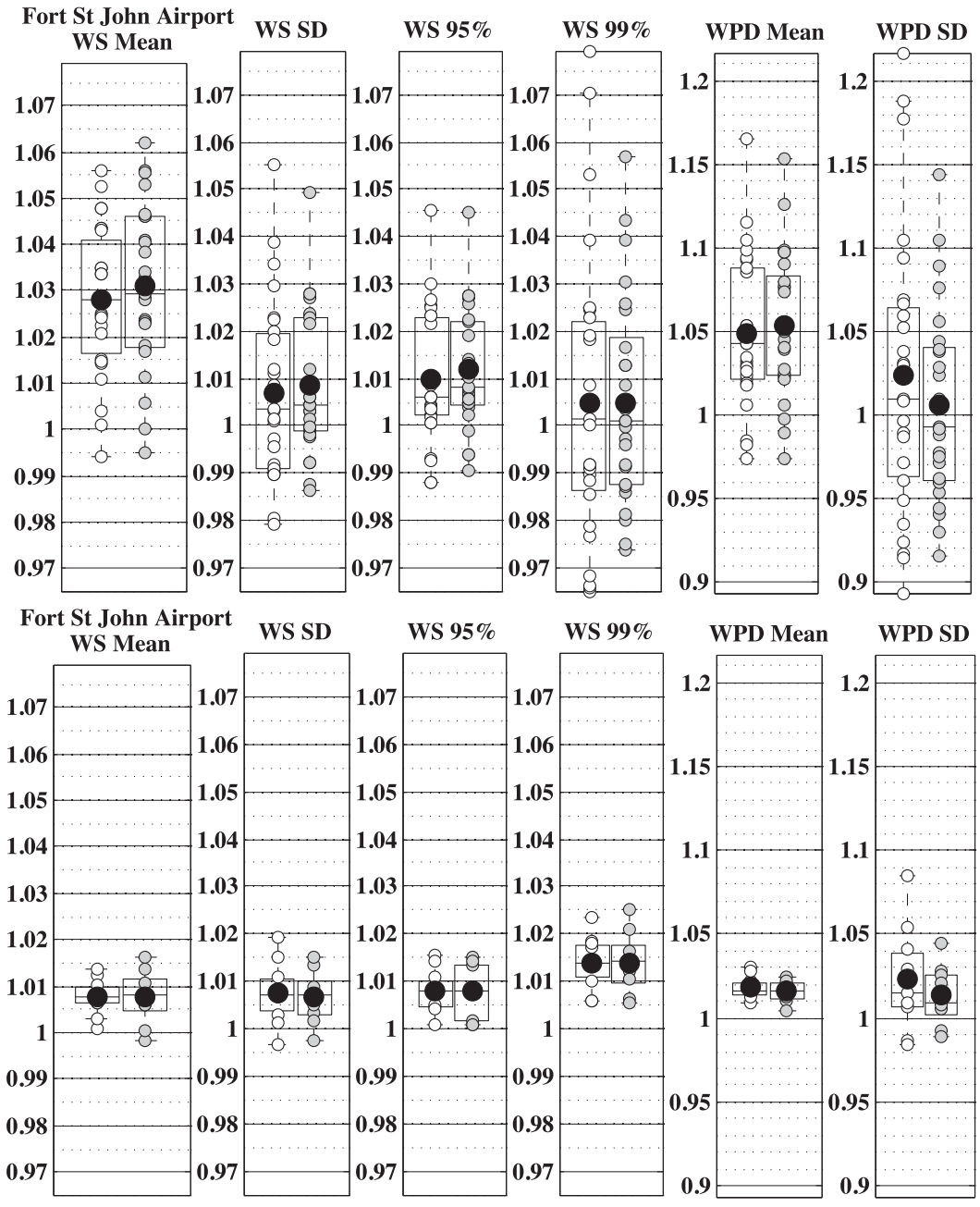

FIG. 5. Box plots showing statistics of ensemble members for 2031–60 for Fort St. John normalized to the 1971–2000 values: (top) CGCM3- and (bottom) ECHAM5-driven simulations. Columns are as in Fig. 4. The white dots represent ensemble members calibrated via the BC pathway, while the gray dots are those calibrated via CF. Black dots, box plots, and the range of vertical axes are as in Fig. 4. Calibrations used corrected station observations.

The differences between calibration pathways can be more clearly seen in Fig. 5, which displays several statistics of the calibrated ensemble members for Fort St. John. Each calibration pathway is shown separately for the CGCM3-driven simulations (top plots) and the ECHAM5-driven simulations (bottom plots). The ensemble means are a measure of the expected change, while the ensemble ranges indicate the robustness of the projected change. In all cases, changes relative to the observed historical period rather than absolute quantities are shown. Similar diagrams for each of the 30 stations are given in Daines (2015). At most stations, the

ensemble ranges for all variables are larger in the top plots (CGCM3 driven) than in the bottom plots (ECHAM5 driven). The range in mean wind speed changes across all stations and all CGCM3-driven ensemble members is −8% to +12%, while that for mean wind power density is −20% to +30%. For ECHAM5-driven ensemble members the corresponding ranges are −4% to +5% in mean wind speed and −14% to +11% in mean wind power density. The results of both calibrations are included. Although the ranges are considerably narrower at individual stations, the overall relationship between the two calibration methods is consistent across all stations.

For Fort St. John, the majority of realizations project increases in wind speed mean, standard deviation, and 95th and 99th percentiles, as well as increased wind power density mean and standard deviation. However, the ensemble spreads of these projected changes are as large as or larger than the ensemble mean change, with many ensemble members predicting decreases of the statistics considered (particularly the standard deviations). The difference between the ensemble means for BC and CF results is small, but the spread of values differs for the two pathways depending upon which statistic is considered. In particular, these results indicate that a small increase in the mean wind speed and power for the period 2031–60 is projected for Fort St. John, but with a small probability that the means could actually decrease. This result holds for both CGCM3- and ECHAM5-driven simulations with both BC and CF calibration pathways. The differences in spread between the two sets of simulations cannot be explained by differences in the number of ensemble members. Randomly subsampling three members from the CGCM3-driven simulations changes the spread of the calibrated changes, but these still differ considerably from the ECHAM5-driven ensemble. As well, averaging successive pairs of 3-hourly CGCM3-driven wind speeds resulted in slight changes insufficient to explain the difference with the 6-hourly ECHAM5 speeds and power. The ECHAM5 and CGCM3 GCMs differ in a number of ways; for example, they have different horizontal and vertical grid resolution, land surface components, and atmosphere–ocean coupling schemes (Randall et al. 2007, section 8.2, table 8.1). These structural differences contribute to the differences noted above; however, further investigation is beyond the scope of this paper.

Maps of the ensemble mean change in wind speed and wind power density for all 30 stations are shown in Fig. 6. Also indicated in this figure is a measure of the robustness of the change, given by the fraction of ensemble member changes with the same sign as the ensemble mean.

In general, both wind speed and power changes associated with the same driving GCM are of the same sign and similar magnitude, although the robustness of this change can be different. The ECHAM5 model projects changes that are generally smaller and less robust than those projected by the CGCM3. At the relatively few locations where robust changes in wind speed are seen in the ECHAM5-driven runs, the sign of the change is often the same in the CGCM3-driven simulations [e.g., in the southern part of the domain, and at Terrace (station 17), Fort St. John (station 5), and Grande Prairie (station 26)]. Differences in ensemble mean changes between calibration pathways are generally small. Our results indicate that according to the CGCM3-driven CRCM, positive and robust relative changes in mean wind speed and wind power density are likely in southern Alberta, northeastern British Columbia, and the nearby region of northwestern Alberta, and also in the coastal region around Terrace (station 17) and Smithers (station 16) near the coast. These large positive changes are not seen in the ECHAM5 projections. Southern British Columbia is likely to experience little change or small decreases. Examining Fig. 6, it is noteworthy that several of the locations showing the largest projected increases in wind speed and wind power density are in regions near existing wind power facilities, such as Fort St. John (station 5) and Lethbridge (station 27).

b. Is calibration of model simulations necessary for determining relative change?

Calibrated projections of future wind speeds can be produced only for locations where observations are available for the calibration. Focusing on mean wind speed and power, we find that relative changes in these quantities are approximately the same for calibrated and uncalibrated changes. This fact will allow us to assess changes in the mean wind speed and power densities across the study domain.

To demonstrate that the calibrated and uncalibrated relative changes are approximately equal, we generated an ensemble of uncalibrated percentage changes in mean wind speed at each station using all possible pairings of 1971–2000 and 2031–60 ensemble members for each of the ECHAM5-driven and the CGCM3-driven simulations. A similar ensemble of relative changes in time-mean wind power density was also computed. A scatterplot of the ensemble means of the relative changes of the calibrated and uncalibrated mean wind speed and mean wind power density (Fig. 7) demonstrates that the results generally lie close to the 1:1 line for each of the BC and CF calibration pathways. The uncalibrated relative changes appear to be a

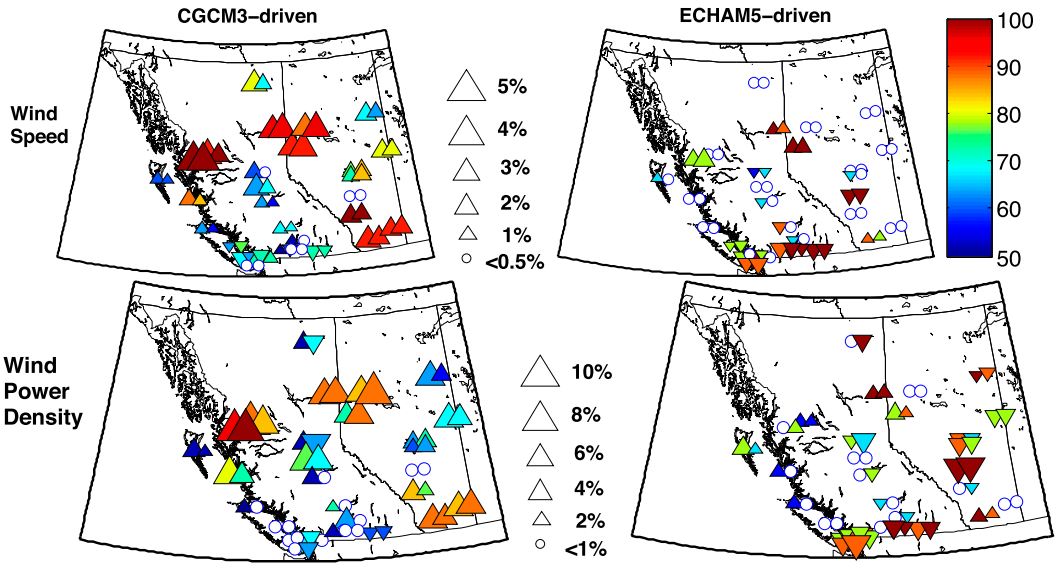

FIG. 6. Map showing the percentage change in the ensemble mean of mean (top) wind speeds and (bottom) wind power density for the calibrated 2031–60 simulations relative to the 1971–2000 simulations at the stations under consideration: (left) CGCM3- and (right) ECHAM5-driven results. The left triangle symbol of each pair of symbols represents the BC pathway at a station, and the right symbol represents the CF pathway. The size of the triangle represents the magnitude of the change, and the vertical vertex of the triangle points in direction of change (positive upward). Note the factor-of-2 increase in the magnitude scale for wind power density. Color represents the percentage of ensemble members with the same sign as the ensemble mean (a measure of robustness). White filled circles represent absolute ensemble mean percentage change of <0.5% in speed and 1% in wind power density with no indication of robustness.

reasonable approximation to the calibrated relative changes at the station locations, although for wind power density the CF-calibrated change is slightly larger than the BC-calibrated change. Additionally, there appears to be a tendency for the uncalibrated relative changes to be slightly larger than the calibrated relative changes when these changes are large, particularly for the ECHAM5-driven simulations.

If calibration is not necessary for estimating the relative future change in mean wind speed and wind power density at the station locations, then future relative changes can be estimated at all CRCM grid points. Maps of ensemble-mean relative changes in wind speed and wind power density are shown in Fig. 8 for both driving models. As was the case for the calibrated relative changes at station locations shown in Fig. 6, over most of the region the ensemble-mean uncalibrated relative changes in mean wind speed and wind power density in the ECHAM5-driven simulations are small decreases or little change as compared with increases in the CGCM3-driven simulations, for example, northeastern Alberta and southwestern British Columbia. Exceptions to this are northern British Columbia, the Rockies, and extreme southern Alberta, where both ensembles show increases. These results indicate that changes in climate may result in slight increases in the wind magnitude where conditions are presently favorable for wind power generation (Fig. 2).

Focusing on relative rather than absolute changes does limit the utility of the results. For example, relative changes do not indicate if a quantity will move above or below a specific threshold such as a 10-m mean wind speed used as an indicator of economically viable power production. Further, the possibility remains that the correspondence between calibrated and uncalibrated relative changes is a result of an unidentified site selection bias; for example, all but one of the stations are at airports, many of which are in valley bottoms or other locations that are not broadly representative of the topography of the region. If observations are available, calibration is possible, and in view of the results presented here, the choice of calibration pathway is not a critical issue.

c. *Robustness and substantiality of estimates of relative change in wind speed and power density*

Focusing on the changes in mean wind speed and wind power density, the projected changes shown in Fig. 5 for Fort St. John were robust in that almost all values showed an increase, but they were not very substantial as the ensemble mean changes were only a few percent. To evaluate the robustness and substantiality of the

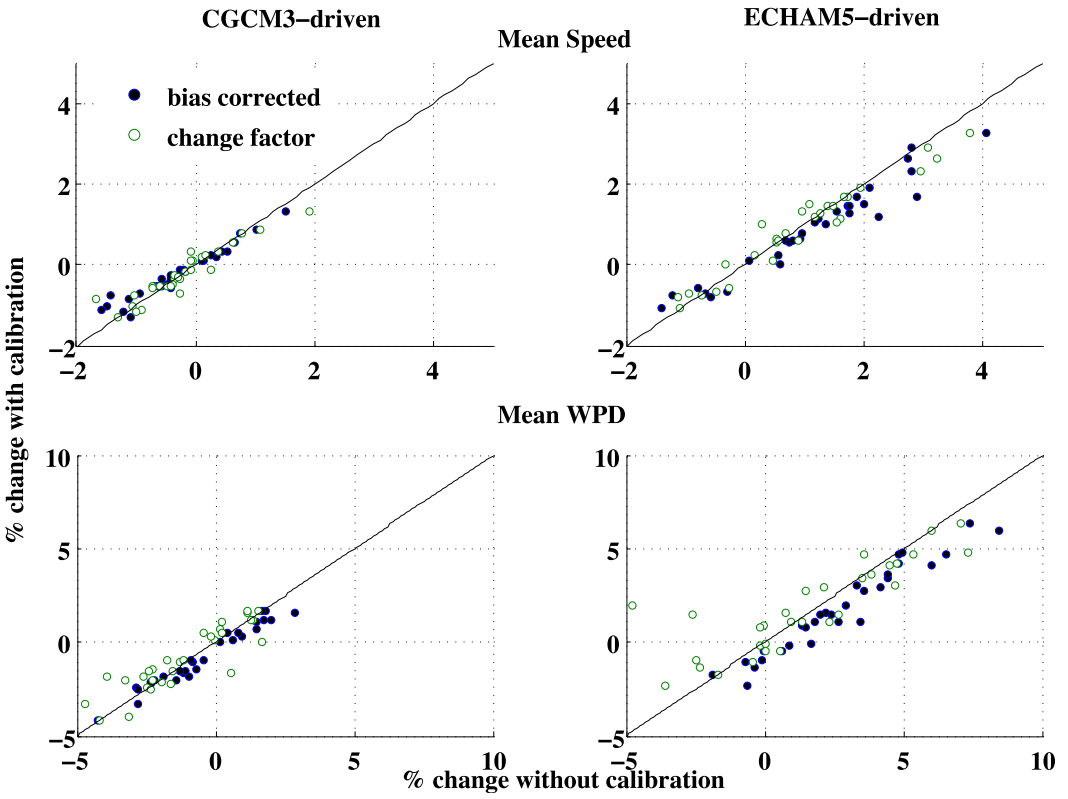

FIG. 7. Scatterplots at the 30 station locations of percentage changes in simulated time-mean (top) wind speeds and (bottom) wind power density at each station calibrated using BC and CF pathways from 1971–2000 to 2031–60 plotted against ensemble mean uncalibrated percentage change for all pairings of 1971–2000 and 2031–60 time-mean wind speeds at the station. A line with a slope of 1 is shown for reference.

relative changes shown in Fig. 8, we quantify robustness by dividing the ensemble-mean change by the ensemble standard deviation. We define the robustness metric R for wind speed as

$$R = \frac{\langle \Delta W_s \rangle}{\sigma_{\text{ens}}(\Delta W_s)},$$

where ΔW_s is difference between the future and past values of the mean speed (or power), $\langle \Delta W_s \rangle$ is the ensemble mean over all ΔW_s, and σ_{ens} is the ensemble standard deviation. For a given $\langle \Delta W_s \rangle$, the larger R is in absolute value, the smaller the difference among ensemble members in the sign and magnitude of the projected change.

We measure the substantiality of the change by the same ensemble-mean change divided by the ensemble-mean temporal standard deviation of the annual-average mean speed (or power):

$$S = \frac{\langle \Delta W_s \rangle}{\langle \sigma_t(W_a) \rangle},$$

where S is the substantiality, W_a are the annual means for each ensemble member, σ_t is the standard deviation of the annual means for each ensemble member, and $\langle \sigma_t(W_a) \rangle$ is ensemble mean of σ_t. Like R, S is a signal-to-noise measure that compares the magnitude of the ensemble mean change in W_s with its characteristic interannual variability.

Maps of robustness of relative wind speed change are shown for both ECHAM5-driven simulations and CGCM3-driven simulations in the top two panels of Fig. 9. The ECHAM5-driven simulations show robust decreases in most parts of Alberta and southern British Columbia as compared with robust increases nearly everywhere in the CGCM3-driven simulations. The GCMs agree along the northern coast and most of northern British Columbia. In particular, both GCMs show robust relative increases in three areas of present wind farms (Fort St. John area, Lethbridge area, and Cape Scott on Vancouver Island), but are not in agreement in the area north of Medicine Hat and east of Calgary and Red Deer in Alberta. For both driving GCMs, the robustness of relative changes in wind power density is similar to that of wind speed (lower panels of Fig. 9).

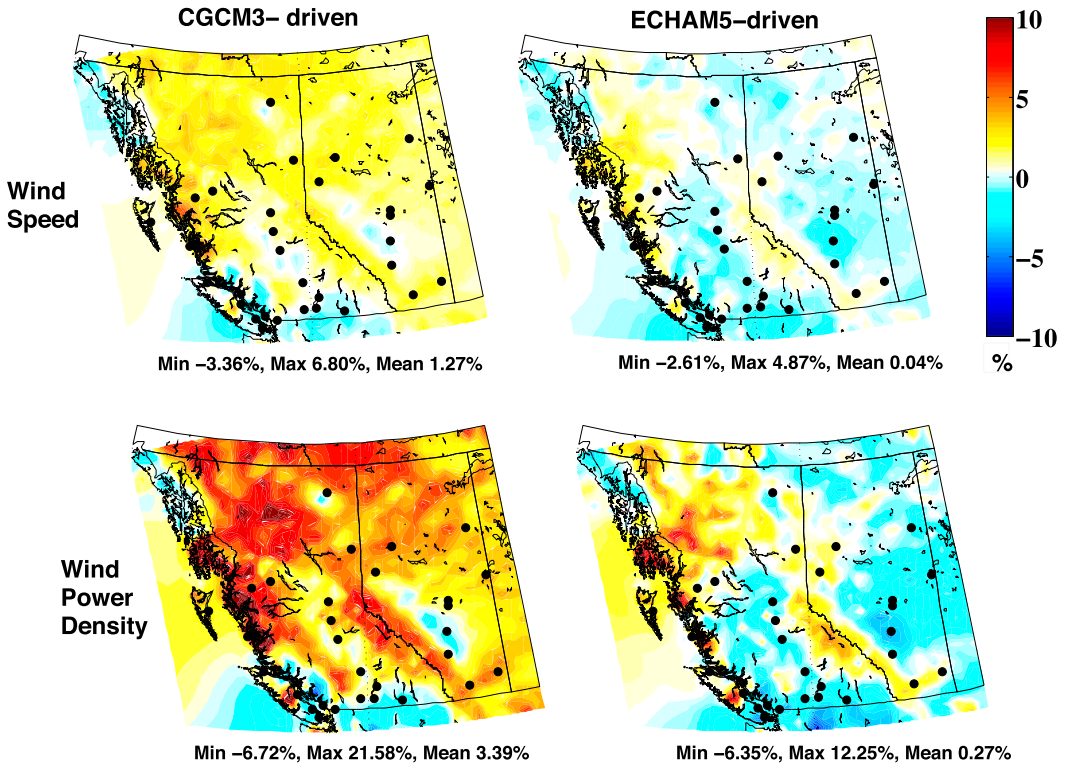

FIG. 8. Percentage relative changes in annual-mean (top) wind speed and (bottom) wind power density from 1971–2000 simulations to 2031–60 simulations using (left) CGCM3- and (right) ECHAM5-driven CRCM smoothed from the original 45-km grid resolution without calibration from observations.

Maps of substantiality are shown for both ECHAM5-driven simulations and CGCM3-driven simulations in Fig. 10. These maps demonstrate that, in general, the projected changes are smaller than the interannual variability, particularly for mean wind speed. Interestingly, although ensemble-mean relative changes for the ECHAM5-driven projections are generally less robust than the CGCM3-driven changes (Fig. 9), along the coast and into central-northern British Columbia they are more substantial (Fig. 10). These results are qualitatively unchanged if substantiality is redefined using the standard deviation of monthly or 3- or 6-hourly averaged winds (Daines 2015).

The results differ quantitatively on a seasonal basis. In a comparison of maps corresponding to Figs. 8–10 for December through February (DJF) and June through August (JJA), the CGCM3-driven simulations show a larger ensemble mean wind power density increase in JJA than the annual ensemble mean, except in central Alberta where there is little change. In DJF, the change is similar to the annual change in the north but is a decrease in the south relative to the annual change. The ECHAM5-driven simulations show larger decreases in both seasons than the annual change. In broad terms, the seasonal results are consistent with those obtained using data from throughout the year. These maps may be found in appendix C of Daines (2015).

5. Discussion

In the introduction, a number of uncertainties in RCM-projected future wind speeds were mentioned briefly. These uncertainties are now considered in more detail.

Calibration of projected changes in wind speed and wind power density used station data that are themselves uncertain, as a result of finite precision instruments and multiple rounding errors introduced by successive unit conversion. In addition, artificial nonstationarities in these data due to changes in measuring equipment or the surrounding environment are not necessarily removed by homogenization (Wan et al. 2010). As for the simulated wind speeds, they have the uncertainties inherent in the differences between the driving GCM, resolution-dependent RCM biases, and as well as natural internal variability across the ensemble members of the RCM. Further, different calibration pathways will generally result in different future projections.

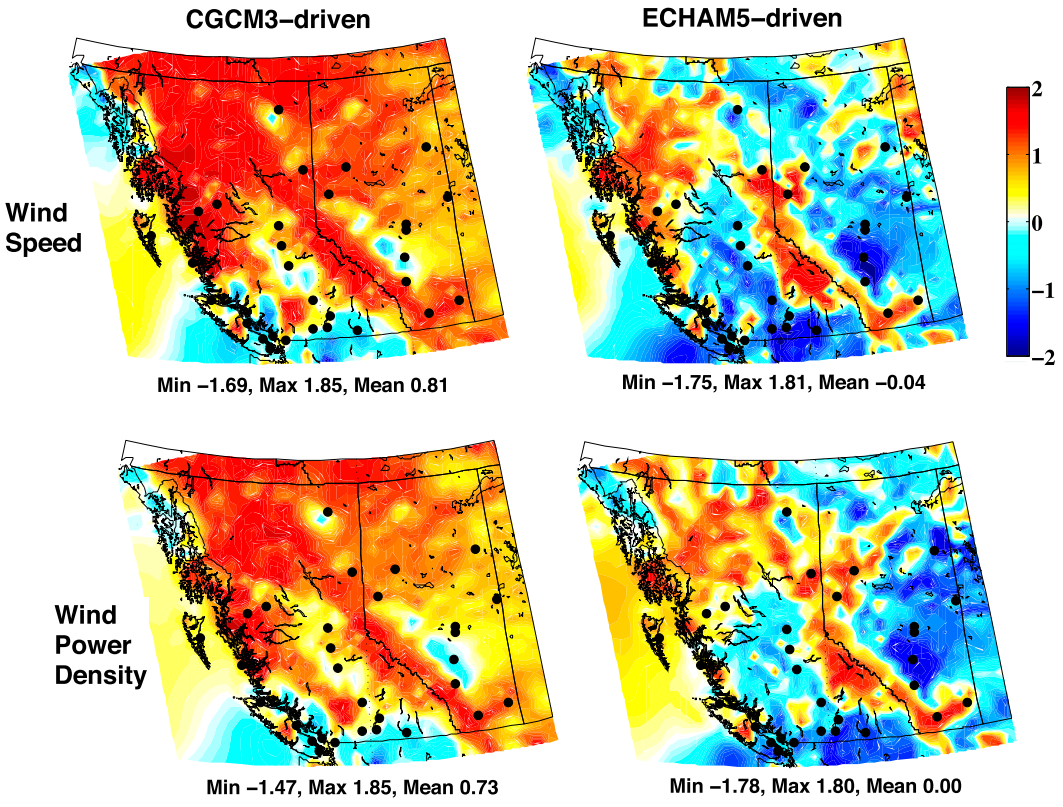

FIG. 9. Robustness R (ensemble relative change in annual-mean wind speed divided by ensemble standard deviation) at each grid point with (left) CGCM3- and (right) ECHAM5-driven simulations.

Station data quality is an issue for the calibrations used in this study. The weather stations at which we have the long-term hourly data needed for both estimation of past climate and calibration of future wind climate were installed at airports to provide information for aviation and not for the purpose of climate research. Wind speeds are sometimes missing or clearly inaccurate because of multiple rounding. In the last few years, this situation seems to have improved with new anemometers installed at all of the stations that continue to operate in the region (NAV Canada 2015). Unfortunately, because of the large interannual variability of wind, using just the last few years of wind speed data is not feasible for calibration purposes or for estimating present-day wind climate. Because the data themselves are uncertain, we cannot quantify the magnitude of the contribution of this uncertainty to projections of future climate. However, as pointed out in section 4b, we can say that projected relative changes in wind speed and power are not strongly tied to these observational uncertainties.

Internal variability in the GCMs used to drive the CRCM and the choice of driving GCM clearly have a large influence on the projected winds. For Fort St. John, the calibrated ensemble mean future wind speed is projected to increase by about 1% for ECHAM5-driven simulations and 3% for CGCM3-driven simulations, but individual ensemble members range anywhere from a slight decrease in mean wind speed to a 7% increase for CGCM3-driven simulations and from a slight decrease to a 2% increase for ECHAM5-driven simulations. The ECHAM5-driven simulations display much less internal variability than the CGCM3-driven simulations, possibly because the ensemble size is smaller.

At Fort St. John, the ensemble spreads are much larger than the differences in ensemble means of the two driving GCMs, so internal variability in the GCMs used to drive the CRCM is a larger contributor to uncertainty than differences in the driving GCM (Fig. 5). This relationship is characteristic of most of the stations considered (Daines 2015).

We are unable to assess the sensitivity of our results to the choice of RCM, as only the CRCM was used. An additional simulation of this model conducted at the higher resolution of 15 km showed only slightly better agreement between the simulated and observed wind speeds at most stations.

For the quantities we have considered, uncertainty due to choice between the two calibration pathways is

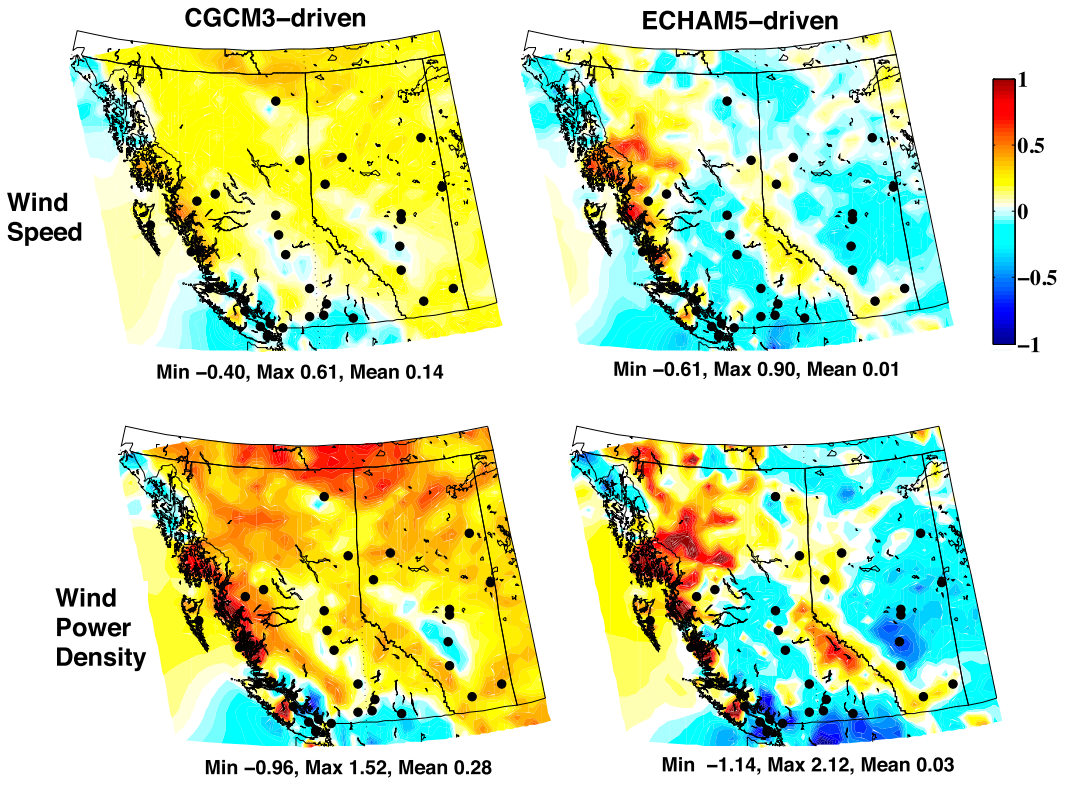

FIG. 10. As in Fig. 9, but for substantiality S (ensemble relative change in annual mean wind speed divided by the ensemble-mean temporal standard deviation of the annual-average means).

small relative to the other uncertainties. This fact is evident in Figs. 5 and 6, where the ensemble means are seen to be similar for both calibration pathways.

In section 4b, we showed that by considering relative rather than absolute changes, one can avoid the need for calibration and uncertainty related to data quality and calibration pathway. However, calibration (bias correction) is still an important and necessary step when using absolute values of climatic variables obtained from climate models. Uncertainties resulting from different driving GCMs and internal variability remain. The second of these, resulting from genuine chaotic behavior in the atmosphere, is both large and irreducible.

6. Conclusions

This study used wind speeds obtained from the dynamical downscaling of global climate simulations to produce climate projections over the western Canadian provinces of British Columbia and Alberta for the period 2031–60, under the SRES-A2 greenhouse gas emissions scenario. This analysis is based on an ensemble of simulations of the Canadian Regional Climate Model driven by both the CGCM3 and ECHAM5 GCMs. These projections were calibrated using historical observations at 30 weather stations within the region.

At the locations of weather stations, only modest changes in the future-projected wind climate are found in the ensemble mean, although, because of variability among the ensemble members, relatively larger changes cannot be ruled out at some stations. Stations near existing wind farms in southwestern Alberta and northeastern British Columbia show small but robust increases in the ensemble mean wind speed (up to 3%) and mean wind power density (up to 5%) for the CGCM3-driven simulations. Smaller increases were projected by the ECHAM5-driven simulations over the same subregions. The same or larger increases are projected at the near-coast stations of Terrace and Smithers, where there are presently no wind farms. At most other stations in the region the projected changes are smaller and in some cases of opposite sign between the CGCM3-driven and ECHAM5-driven simulations.

We found that while relative changes in the ensemble means of projected changes were sensitive to the driving GCM, the internal variability between the members of each ensemble resulted in the largest uncertainties, with the variability much higher for CGCM3 than for ECHAM5. The results were only weakly sensitive to the

calibration pathway used. The data used for calibration are themselves uncertain, but we are unable to quantify this uncertainty.

Having demonstrated that the ensemble-mean relative changes of wind speed and power at the station locations are similar for both calibrated and uncalibrated projections, uncalibrated relative changes in future wind climate across the RCM domain were produced. In general, relative changes appear to be reasonably robust, but not very substantial when compared with the range of annual variability, and generally in good general agreement with the results at individual stations. While the anthropogenically forced change (as estimated by the ensemble mean) is small, the possibility remains of reasonably large increases—or small decreases—in both wind speed and wind power density occurring as a result of natural internal variability. The large range of projected changes for individual simulations (e.g., −20% to +30% for wind power density over all stations) reinforces the important role of internal variability in climate change projections as highlighted by Deser et al. (2012).

The results of this study may be of interest to those planning to install or expand wind farms in the region as the overall projection is that large changes are not likely. Specifically, only small increases are likely in the areas that are presently being developed for wind farms. Uncertainty in projected absolute changes in wind speed and wind power density could be reduced by using better-quality station observations in the calibration procedure, but this is not the major contributor to the overall uncertainty in wind projections. Rather, it is the irreducible uncertainties of internal climate variability and structural differences among driving GCMs that appear to play a dominant role.

Acknowledgments. Partial funding was provided by the Pacific Institute for Climate Solutions via a graduate fellowship to JD. CRCM simulations were conducted by the Ouranos Consortium and the University of Victoria as part of the Natural Sciences and Engineering Research Council of Canada (NSERC) Collaborative Research and Development project, "Dynamical Downscaling of Western and Eastern Canadian Hydroclimate" (CRDPJ 403886-10), which provided funding to CC. AM acknowledges support from NSERC. The authors thank Michel Giguère (Ouranos Consortium) for running the simulations, and Mourad Labassi (Ouranos Consortium), Ed Wiebe (University of Victoria), and Jean des Rosiers for technical support. Tom Pedersen, David Atkinson, and three anonymous reviewers are also acknowledged for their helpful comments.

REFERENCES

Alberta Energy, 2015: Electricity statistics. Accessed 8 July 2015. [Available online at http://www.energy.alberta.ca/Electricity/682.asp.]

Amante, C., and B. Eakins, 2009: ETOPO1 1 arc-minute global relief model: Procedures, data sources and analysis. NOAA Tech. Memo. NESDIS NGDC-24, 25 pp., accessed 5 March 2015. [Available online at https://www.ngdc.noaa.gov/mgg/global/relief/ETOPO1/docs/ETOPO1.pdf.]

Breslow, P. B., and D. J. Sailor, 2002: Vulnerability of wind power resources to climate change in the continental United States. *Renewable Energy*, **27**, 585–598, doi:10.1016/S0960-1481(01)00110-0.

Canadian Wind Energy Association, 2015: Installed capacity. Accessed 8 July 2015. [Available online at http://canwea.ca/wind-energy/installed-capacity/.]

Casati, B., and R. de Ela, 2014: Temperature extremes from Canadian Regional Climate Model (CRCM) climate change projections. *Atmos.–Ocean*, **52**, 191–210, doi:10.1080/07055900.2014.886179.

Caya, D., and R. Laprise, 1999: A semi-implicit semi-Lagrangian regional climate model: The Canadian RCM. *Mon. Wea. Rev.*, **127**, 341–362, doi:10.1175/1520-0493(1999)127<0341:ASISLR>2.0.CO;2.

Culver, A., and A. Monahan, 2013: The statistical predictability of surface winds over western and central Canada. *J. Climate*, **26**, 8305–8322, doi:10.1175/JCLI-D-12-00425.1.

Curry, C. L., D. van der Kamp, and A. H. Monahan, 2012: Statistical downscaling of historical monthly mean winds over a coastal region of complex terrain. I. Predicting wind speed. *Climate Dyn.*, **38**, 1281–1299, doi:10.1007/s00382-011-1173-3.

——, B. Tencer, K. Whan, A. J. Weaver, M. Giguère, and E. Wiebe, 2016a: Searching for added value in simulating climate extremes with a high-resolution regional climate model over western Canada. *Atmos.–Ocean*, doi:10.1080/07055900.2016.1158146, in press.

——, ——, ——, ——, ——, and ——, 2016b: Searching for added value in simulating climate extremes with a high-resolution regional climate model over western Canada. II. Basin-scale results. *Atmos.–Ocean*, doi:10.1080/07055900.2016.1215287, in press.

Daines, J. T., 2015: Present and future wind energy resources in western Canada. M.Sc. thesis, School of Earth and Ocean Sciences, University of Victoria, 155 pp. [Available online at https://dspace.library.uvic.ca/handle/1828/6703?show=full.]

Deser, C., R. Knutti, S. Solomon, and A. S. Solomon, 2012: Communication of the role of natural variability in future North American climate. *Nat. Climate Change*, **2**, 775–779, doi:10.1038/nclimate1562.

Diaz-Nieto, J., and R. L. Wilby, 2005: A comparison of statistical downscaling and climate change factor methods: Impacts on low flows in the River Thames, United Kingdom. *Climatic Change*, **69**, 245–268, doi:10.1007/s10584-005-1157-6.

Eagland, N., 2015: B.C.'s wind-power projects stuck in doldrums, industry players say, as province pushes Site C dam. *Province*, 12 April. [Available online at http://canwea.ca/b-c-s-wind-power-projects-stuck-in-doldrums-industry-players-say-as-province-pushes-site-c-dam/.]

EnergyBC, 2016: Where our electricity comes from. Accessed 14 September 2016. [Available online at http://www.energybc.ca/map/bcenergymap.html.]

Haerter, J. O., S. Hagemann, C. Moseley, and C. Piani, 2011: Climate model bias correction and the role of timescales. *Hydrol. Earth Syst. Sci.*, **15**, 1065–1079, doi:10.5194/hess-15-1065-2011.

Ho, C. K., D. B. Stephenson, M. Collins, C. A. T. Ferro, and S. J. Brown, 2012: Calibration strategies: A source of additional uncertainty in climate change projections. *Bull. Amer. Meteor. Soc.*, **93**, 21–26, doi:10.1175/2011BAMS3110.1.

Laprise, R., 2008: Regional climate modelling. *J. Comput. Phys.*, **227**, 3641–3666, doi:10.1016/j.jcp.2006.10.024.

Mansbach, D. K., and D. R. Cayan, 2010: Statistical downscaling of wind for California wind farms with an application to 21st century climate change scenarios. *First Conf. on Weather, Climate, and the New Energy Economy*, Atlanta, GA, Amer. Meteor. Soc., J5.3. [Available online at https://ams.confex.com/ams/90annual/techprogram/paper_161348.htm.]

Manwell, J. F., J. G. McGowan, and A. L. Rogers, 2012: Aerodynamics of wind turbines. *Wind Energy Explained: Theory, Design and Application*, John Wiley and Sons, 84–88.

Mesinger, F., and Coauthors, 2006: North American Regional Reanalysis. *Bull. Amer. Meteor. Soc.*, **87**, 343–360, doi:10.1175/BAMS-87-3-343.

Michelangeli, P.-A., M. Vrac, and H. Loukos, 2009: Probabilistic downscaling approaches: Application to wind cumulative distribution functions. *Geophys. Res. Lett.*, **36**, L11708, doi:10.1029/2009GL038401.

Mladjic, B., L. Sushama, M. Khaliq, R. Laprise, D. Caya, and R. Roy, 2011: Canadian RCM projected changes to extreme precipitation characteristics over Canada. *J. Climate*, **24**, 2565–2584, doi:10.1175/2010JCLI3937.1.

Monahan, A. H., 2014: Wind speed probability distribution. *Encyclopedia of Natural Resources*, Taylor and Francis, 1084–1088.

Nakićenović, N., and R. Swart, Eds., 2000: *Special Report on Emissions Scenarios*. Cambridge University Press, 570 pp.

National Renewable Energy Laboratory, 2014: Wind data details. Dynamic maps, GIS data, and analysis tools (updated 6 February 2014). Accessed 5 March 2015. [Available online at http://www.nrel.gov/gis/wind_detail.html.]

NAV Canada, 2015: Techwatch. Winter 2015 ed., 16 pp., accessed 28 June 2015. [Available online at http://www.navcanada.ca/EN/media/Publications/TECHWATCH%20-%20Winter%202015.pdf.]

Piani, C., G. P. Weedon, M. Best, S. Gomes, P. Viterbo, S. Hagemann, and J. O. Haerter, 2010: Statistical bias correction of global simulated daily precipitation and temperature for the application of hydrological models. *J. Hydrol.*, **395**, 199–215, doi:10.1016/j.jhydrol.2010.10.024.

Plummer, D. A., and Coauthors, 2006: Climate and climate change over North America as simulated by the Canadian RCM. *J. Climate*, **19**, 3112–3132, doi:10.1175/JCLI3769.1.

Pryor, S. C., J. T. Schoof, and R. J. Barthelmie, 2005: Climate change impacts on SWS and wind energy density in northern Europe: Empirical downscaling of multiple AOGCMs. *Climate Res.*, **29**, 183–198, doi:10.3354/cr029183.

——, and Coauthors, 2009: Wind speed trends over the contiguous United States. *J. Geophys. Res.*, **114**, D14105, doi:10.1029/2008JD011416.

——, R. J. Barthelmie, and J. T. Schoof, 2012: Past and future wind climates over the contiguous USA based on the North American Regional Climate Change Assessment Program model suite. *J. Geophys. Res.*, **117**, D19119, doi:10.1029/2012JD017449.

Randall, D. A., and Coauthors, 2007: Climate models and their evaluation. *Climate Change 2007: The Physical Science Basis*, S. Solomon et al., Eds., Cambridge University Press, 589–662.

Rasmussen, D. J., T. Holloway, and G. F. Nemet, 2011: Opportunities and challenges in assessing climate change impacts on wind energy—A critical comparison of wind speed projections in California. *Environ. Res. Lett.*, **6**, 024008, doi:10.1088/1748-9326/6/2/024008.

Sailor, D. J., M. Smith, and M. Hart, 2008: Climate change implications for wind power resources in the northwest United States. *Renewable Energy*, **33**, 2393–2406, doi:10.1016/j.renene.2008.01.007.

Salathé, E. P., R. Steed, C. F. Mass, and P. H. Zahn, 2008: A high-resolution climate model for the U.S. Pacific Northwest: Mesoscale feedbacks and local responses to climate change. *J. Climate*, **21**, 5708–5726, doi:10.1175/2008JCLI2090.1.

Scorah, H., A. Sopinka, and G. C. van Kooten, 2012: The economics of storage, transmission and drought: Integrating variable wind power into spatially separated electricity grids. *Energy Econ.*, **34**, 536–541, doi:10.1016/j.eneco.2011.10.021.

Sopinka, A., 2012: Assessing the impacts of wind integration in the western provinces. Ph.D. thesis, University of Victoria, 184 pp.

Tye, M. R., D. B. Stephenson, G. J. Holland, and R. W. Katz, 2014: A Weibull approach for improving climate model projections of tropical cyclone wind-speed distributions. *J. Climate*, **27**, 6119–6133, doi:10.1175/JCLI-D-14-00121.1.

Wan, H., X. L. Wang, and V. R. Swail, 2010: Homogenization and trend analysis of Canadian near-surface wind speeds. *J. Climate*, **23**, 1209–1225, doi:10.1175/2009JCLI3200.1.